Bulgarian Chemical Communications, Volume 50, Special issue H (pp. 122–129) 2018

Characterisation of mechanochemically synthesised N-doped TiO_2

N. G. Kostova*[,1], M. Fabian[2], E. Dutkova[2], M. Balaz[2], M. Shipochka[3]

[1] *Institute of Catalysis, Bulgarian Academy of Sciences, 1113 Sofia, Bulgaria*
[2] *Institute of Geotechnics, Slovak Academy of Sciences, 04001 Kosice, Slovakia*
[3] *Institute of General and Inorganic Chemistry, Bulgarian Academy of Sciences, 1113 Sofia, Bulgaria*

Received: January 29 2018; Revised: March 20, 2018

N-doped TiO_2 photocatalyst (P25-u) was prepared by combined mechanochemical/thermal synthesis. Urea was used as nitrogen source. Wet grinding experiments have been conducted on titanium dioxide P25 Degussa in a high-energy planetary mill. As-milled samples were calcined at 400 °C. The samples were characterised by X-ray diffraction (XRD), N_2 adsorption-desorption isotherms, UV-vis diffuse reflectance spectroscopy (DRS), X-ray photoelectron spectroscopy (XPS), and photoluminescence spectroscopy (PL) analysis. XRD results showed that art of phase anatase transforms to rutile during wet milling. All XRD peaks were broadened indicating that the crystallite size was within the nanometre range. P25-u samples possessed lower S_{BET} values than the initial P25 Degussa. Milling in the wet environment resulted in deterioration of the porous structure. A lower photoluminescence intensity of mechanochemically synthesised P25-tu samples in comparison with the initial P25 ones indicated a lower recombination rate of photoexcited electrons and holes. Estimated E_{bg} value for P25-u was 2.36 eV. This result suggests a possibility to apply as-prepared material as a photocatalyst in degradation process with visible light irradiation. Mechanochemically synthesised N-doped TiO_2 samples using urea exhibited a higher decolourisation rate of Methyl Orange dye than the commercially available TiO_2 Degussa powder under visible light irradiation.

Key words: mechanochemistry, photocatalysis, titanium dioxide, N-doping, Methyl Orange, photoluminescence.

INTRODUCTION

Titanium dioxide has been widely investigated because of its low cost, good physical and chemical stability, and environmental compatibility [1]. TiO_2 absorbs only a small fraction of the solar spectrum emission due to its band gap energy value. Photocatalysts that can exhibit high reactivity under visible light should be developed to use the main part of the solar spectrum. Thus, anion-doped TiO_2 has attracted considerable attention due to its manifested activity under visible light. Among all, N-doped TiO_2 seems to be a promising photocatalyst [2]. Different techniques have been used for doping titania with non-metal ions, e.g. sol-gel technology [3], magnetron sputtering deposition method [4], chemical vapour deposition [5], decomposition of N-containing metal organic precursors [6,7], etc. Nitrogen can be doped into titania by using different organic compounds, e.g. Refs. [8−10].

Commercially available TiO_2 (Degussa P 25), which is a standard material in the field of photocatalytic reactions, contains anatase and rutile phases [11]. The rutile phase with a band gap of 3.0 eV is the most thermodynamically stable form of crystalline titania, while anatase with band gap of 3.2 eV is a metastable form of TiO_2. The presence of rutile in the samples reduces the recombination effect toward enhancing the photocatalytic performance in comparison with pure single phase of titania [12]. Anatase absorption affinity for organic compounds is higher than that of rutile [13]. This phase exhibits lower rates of recombination in comparison with rutile due to its higher rates of hole trapping [14]. The anatase is generally regarded as the more photochemical active phase of titania, presumably due to the combined effect of lower rate of recombination and higher surface adsorption capacity.

Mixed-phase materials (A+R) exhibit a higher photocatalytic activity than either pure phase alone [15]. Due to the higher activity of pure-phase anatase compared to rutile, anatase is conventionally considered the active component in mixed-phase catalysts with rutile serving passively as an electron sink. These mixed-phase materials exhibit increased photo-efficiencies and are activated by lower energy light [16].

In this study, pure and N-doped TiO_2 P25 Degussa as possible photocatalysts were studied. As-prepared samples were synthesised by a mechanochemical approach. Urea was used as nitrogen source. Photodecomposition of Methyl orange (MO) under visible light irradiation was used as a model reaction. An improved photocatalytic activity was

* To whom all correspondence should be sent
E-mail: nkostova@ic.bas.bg

found for all N-doped TiO_2 Degussa P25 samples. The aim of the present study was to investigate the influence of doping and of the local structure variation of titania on its photocatalytic properties.

EXPERIMENTAL

Mechanochemical synthesis

Commercial TiO_2 P25 (Degussa, Holand) and urea of analytical grade were used without further purification. N-doped TiO_2 samples were prepared by addition of urea as modifier to TiO_2 P25 Degussa by mechanochemical/thermal synthesis using a high-energy planetary ball mill Pulverisette 6 (Fritsch, Germany). Titania powder was mixed with 5 wt.% urea before being placed in the reactor vessel. Wet milling was performed in presence of 1.2 ml distilled water. The sample was milled for 30 min at 550 rpm under argon using a chamber (250 cm^3 in volume) with 21 balls (10 mm in diameter) both made of zirconia. The ball-to-powder mass ratio was 40:1. To remove residual urea, the yellowish sample of N-doped TiO_2 P25 Degussa was calcined at 400 ^oC in air for 1 h. According to urea modifier, the N-doped samples were denoted as P25-u. An original TiO_2 P25 powder was also used as a reference sample (P25).

Characterisation techniques

The crystal structure was characterised by using a D8 Advance X-ray diffractometer (Bruker, Germany) in the Bragg-Brentano geometry working with a CuK_α radiation (λ = 0.15406 nm) and a scintillation detector. Data were collected over the angular range of $20^o < 2\theta < 65^o$ with scanning steps of 0.020^o and a measurement step time interval of 9 s. For data processing, commercial Bruker tools were used. Specifically, Diffrac^{plus} Eva database was utilised for phase identification.

A nitrogen adsorption apparatus NOVA 1200e Surface Area & Pore Size Analyzer (Quantachrome Instruments, United Kingdom) was employed to record adsorption-desorption isotherms. Specific surface area (S_{BET}) values were calculated using Brunauer-Emmett-Teller (BET) equation. The pore size distribution was calculated using the Barrett-Joyner-Halenda (BJH) method. The measurements were performed at the liquid nitrogen temperature.

Diffuse reflectance UV-vis spectra for evaluation of photophysical properties were recorded in the diffuse reflectance mode (R) and transformed to absorption spectra through the Kubelka-Munk function [17]. A Thermo Evolution 300 UV-vis spectrophotometer (Thermo Scientific, USA) equipped with a Praying Mantis device with Spectralon as the reference was used. Reflectance data were obtained as a relative percentage reflectance to a non-absorbing material (spectralon) which could optically diffuse light.

Sample composition and electronic structure were investigated by X-ray photoelectron spectroscopy (XPS). The measurements were carried out on an AXIS Supra electron - spectrometer (Kratos Analitycal Ltd., Japan) using monochromatic AlK_α radiation with photon energy of 1486.6 eV and charge neutralisation system. Binding energies (BE) were determined with an accuracy of ±0.1 eV. The chemical composition of the films was determined by monitoring the areas and binding energies of C1s, O1s, and Ti2p photoelectron peaks using an asymmetric Gaussian-Lorentzian function fit. Applying commercial data-processing software of Kratos Analytical Ltd. concentrations of the different chemical elements (as atomic %) were calculated by normalising the areas of the photoelectron peaks to their relative sensitivity factors.

Photoluminescence (PL) spectra at room temperature were acquired at right angle on a photon counting spectrofluorometer PC1 (ISS, USA) with a photoexcitation wavelength of 325 nm. A 300-W xenon lamp was used as the excitation source. For measuring the PL intensity, the powders were suspended in absolute ethanol.

Sample photocatalytic activity in the reaction of Methyl orange decolourisation was measured under visible light illumination. The photocatalytic experiments were carried out in a semi-batch photoreactor equipped with a magnetic stirrer as reported in previous work [18]. Methyl Orange dye was used as reactant with a concentration of 10 mg/L. The suspension was prepared by adding N-doped TiO_2 sample (100 mg) to 100 ml of Methyl Orange solution. MO degree of decolourisation could be easily monitored by optical absorption spectroscopy. Prior to deposition, the suspension of MO with N-doped TiO_2 was sonicated for 5 min to obtain an optimally dispersed system using an UP200S ultrasound processor (Hielscher, Germany) at 24 Hz in a pulse mode. The suspension was magnetically stirred in the dark for 30 min to ensure an adsorption-desorption equilibrium. Then the light was turned on and this was considered to be the initial moment (t = 0 s) of the photocatalytic reaction. The suspension was irradiated by a Philips TUV lamp (4 W) at UV-C monochromatic radiation (λ = 254 nm). All experiments were performed at a constant stirring rate of 400 rpm at room temperature. During the photo-catalytic reaction the concentration of MO was determined by monitoring the changes of the main absorbance peak at λ = 463 nm. MO decolourisation reaction course

was monitored after aliquot sampling at regular time intervals. Each aliquot sample was returned to the reaction mixture immediately after spectrophotometric measurement (operation under constant volume) and the illumination was switched on again.

RESULTS AND DISCUSSION

X-ray data analysis

Powder XRD patterns of initial TiO_2 P 25 as well as of ball-milled and N-doped TiO_2 P 25 Degussa nanopowders are presented in Fig. 1. Diffraction peaks due to anatase and rutile (for the P25 and P25-u samples) are clearly observed. All XRD peaks are broadened indicating that crystallite sizes were within the nanometre range. Anatase transformation to rutile phase during ball milling was in agreement with a study of Begin-Colin *et al*. [19]. Phase content of the particular samples was calculated from the integrated intensity of the anatase (101) and rutile (110) peaks. The mass fraction of anatase (W_a) and rutile (W_r) could be calculated from

$$W_a = K_a A_a/(K_a A_a + A_r) \text{ and} \quad (1)$$

$$W_r = A_r/(K_a A_a + A_r), \quad (2)$$

where A_a and A_r are the integrated intensities of the anatase (101) and rutile (110) peaks, respectively. W_a and W_r represent the weight fractions of anatase and rutile, respectively. The optimised correction coefficient K_a has a value of 0.886 [20].

Fig. 1 illustrates that the relative peak intensities ascribed to a rutile phase increased from P25 to P25-u, to indicate more progression of anatase transformation to rutile phase. Sample crystallite sizes were calculated using the Debye-Scherrer equation [21]. They are given in Table 1. From Rietveld analysis of XRD data, it can be deduced that the anatase/rutile ratio was changed and the average crystallite size decreased after doping. All diffracttion peaks were broadened because of the nanosize crystals [22] as well as due to structural disorder introduced by milling procedure [23].

Specific surface area

The specific surface area (S_{BET}) values for all the studied samples are listed in Table 1. It is known that specific surface area is an important factor influencing activity of TiO_2 particles [24]. The specific surface area of the standard sample P25 was 52 m^2/g in good agreement with [25]. The sample P25-u possessed lower S_{BET} value indicating that milling in the wet environment resulted in deterioration of the porous structure. In our experiments distilled water was in the wet milling process. The reduction of S_{BET} value for TiO_2 upon milling was also reported in [26] and the lowest value was registered for the wet-milled sample in methanol. The adsorption-desorption isotherms of two samples were recorded in whole p/p_0 interval to examine the surface properties in more detail (Fig. 2).

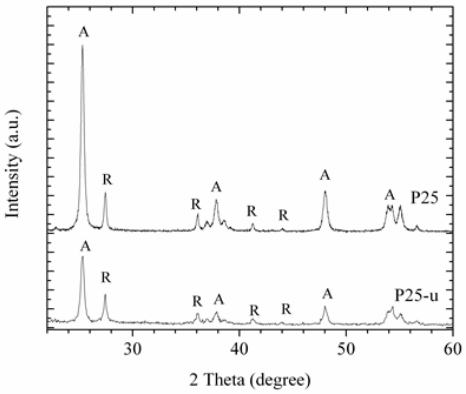

Fig. 1. XRD patterns of initial P25 and P25-u.

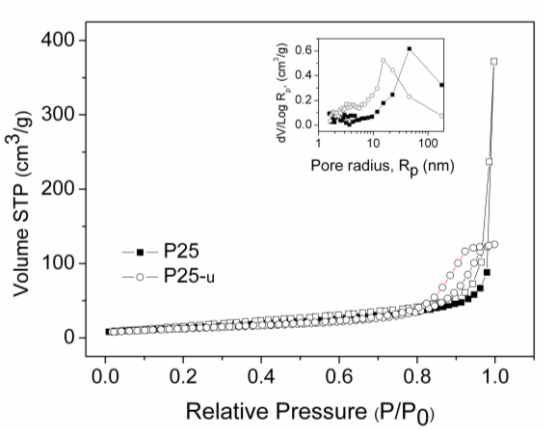

Fig. 2. N_2 adsorption-desorption isotherms of all samples (full shapes correspond to the adsorption curve and empty ones to the desorption curve) and Pore size distribution calculated from the N_2 desorption isotherm (insert).

Table 1. Sample composition (A = anatase and R = rutile); phase composition, average crystalline size; BET surface area, band gap (E_g), chemical composition obtained by XPS, and the reaction rate constant (k') of P25 reference and mechanochemically synthesized samples.

Sample	Phase, %		Crystallite size, nm		S_{BET}, m^2g^{-1}	Band gap, eV	Chemical composition at.%			$k \times 10^2$ min^{-1}
	A	R	A	R			Ti	O	N	
P 25	82	18	24	34	52	3.2	31.6	68.4	-	0.3
P25-u	70	30	20	30	38	2.36	31.9	68.0	0.1	9.4

It can be seen that all isotherms contain a hysteresis loop, which is evidence for presence of mesopores in their structures. P25 sample isotherm shape in the area of relative pressures around 1 hints to the presence of macropores. According to the classification of Sing *et al*. [27] the shape of the isotherm is on the borderline between types II and IV. The isotherm of the P25-u sample fits into type IV. The hysteresis loop can be classified as H3. Analysis of the pore size distribution (Fig. 2 insert) provided further information on pore types.

It can be seen that the pore size distribution of the P25-u sample is significantly different. Whereas the P25 sample contains mainly big mesopores and macropores, the P25-u sample is almost completely mesoporous. Smaller pores with maximum in pore radius distribution around 8 nm were observed with P25-u sample. Its pore size distribution profile is similar to that reported in Ref. [28].

XPS analysis

Samples were also analysed by XPS to evaluate the surface chemical species taking into account both the Ti2p and O1s regions. The latter allows investigation of both quality and abundance of OH surface species, which is fundamental in the photocatalytic process [29]. XPS survey spectra of initial P25 and P25-u are displayed in Fig. 3a. The binding energies were calibrated with respect to the C1s peak at 284.5 eV. XPS analysis showed that the P25 and P25-u particles had C, O, and Ti elements on their surface. Moreover, N element was also present because of P25 co-milling with urea. The chemical composition of the samples is given in Table 1.

Ti $2p_{1/2}$ and Ti $2p_{3/2}$ spin orbital splitting photoelectrons of both samples were localised at binding energies of 464.8 and 459 eV, respectively, as seen in Fig. 3c. A peak separation value of 5.8 eV between the $Ti2p_{1/2}$ and $Ti2p_{3/2}$ signals is in agreement with literature data on Ti^{4+} [30,31]. No peaks of titanium oxidation state other than 4+ were found in the spectrum of the P25-u sample. The absence of broad and shoulder peaks made it reasonable to conclude that only Ti^{4+} species was bonded to O^{2-} in the TiO_2 lattice on the surface.

The shape of the O1s peaks in the XPS spectra of both P25 and P25-u samples are similar and have a slight asymmetry at the higher binding energy side of the peaks. The O1s peaks could be deconvoluted in two components (Fig. 3b). The component of lower binding energy at ~530.2 eV is attributed to oxygen bonded to tetravalent Ti ions ($Ti\text{-}O_L$), whereas that of ~531.4 eV is ascribed to oxygen atoms in hydroxyl groups [32].

Diffuse reflectance spectra

Diffuse-reflectance spectra (DRS) in both the ultra-violet and visible ranges were recorded in order to investigate the optical properties of as-prepared samples as shown in Fig. 4. The TiO_2 P25 Degussa sample has a wide absorption band in the range from 200 to 380 nm (see Fig. 4). An absorption edge for the mechanically activated TiO_2 P25 Degussa is red shifted and the absorption tail is extended to 420 nm. The yellowish N-doped mechanochemically synthesised P25-u sample shows two absorption edges at around 408 nm and 550 nm. The former edge is the same as for P25 after mechanical activation. The latter edge seems to indicate the formation of a new N2p-based band, which is located above the O2p-based valence band [33].

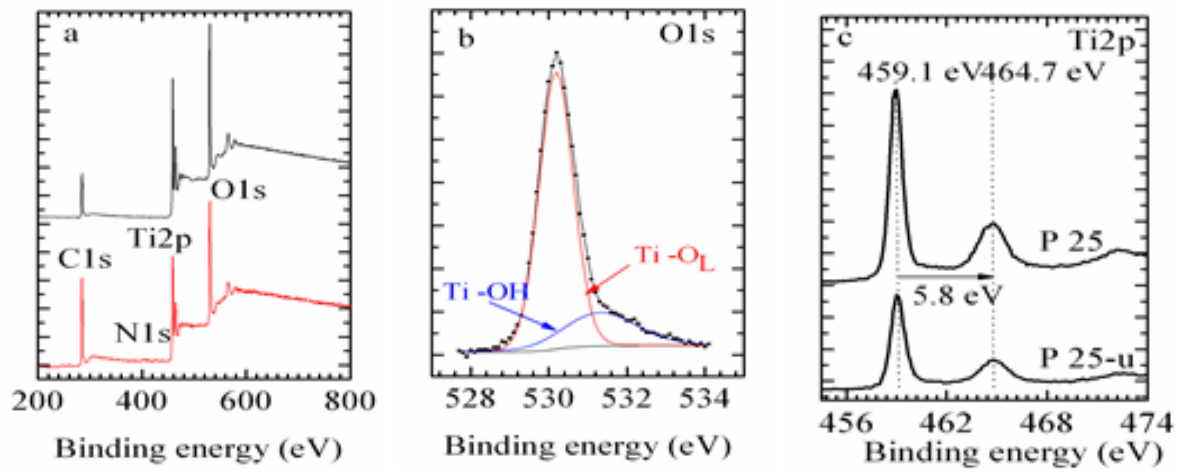

Fig. 3. XPS survey spectra of initial P25 and P25-u (a), XPS collected from P25 and P25-u samples for O1s (b) and Ti2p (c) core levels.

N-doping resulted in an intense increase in absorption in the visible light region and a red shift in the absorption edge of TiO_2 P25. Mixing of the N2p states with the valence band of TiO_2 was found to contribute to an increase of the valence band [34]. This led to band gap narrowing in the N-doped sample mechanochemically synthesised using urea.

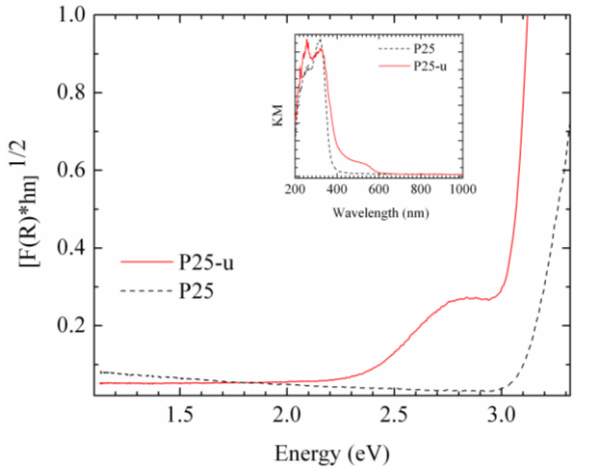

Fig. 4. DRS spectra of initial P25 and P25-u samples and corresponding Tauc's plot (insert).

In addition, the UV-vis diffuse reflectance spectroscopy was employed to estimate the band gap energies of as-prepared samples. Band gap values were calculated using the UV-vis spectra from the following equation:

$$\alpha(h\nu) = A(h\nu - E_{bg})^{½}, \quad (3)$$

where α is the absorption coefficient and *hν* is the photon energy. The band gap energies were calculated by extrapolating a straight line to the abscissa axis. The value of hν extrapolated to α = 0 gives an absorption energy, which corresponds to a band gap energy. Sample band gaps obtained through Kubelka-Munk plots are listed in Table 1. A value of 3.20 eV was found for initial P25. The mechanically activated TiO_2 P25 Degussa has energy band gap E_{bg} = 3.05 eV (Fig. 4). Narrowing of the band gap was observed after modification of P25 with urea.

Furthermore, a new band with maximum at 2.9 eV appeared in the spectra of P25-u samples. The estimated E_{bg} value for P25-u was 2.36 eV. The red shift is attributed to creation of additional electronic states in the band gap of TiO_2 P25 [35]. These results suggest a possible application of the as-prepared material as a photocatalyst for degradation process with lower energetic requirements than TiO_2.

Photoluminescence

The PL behaviour of TiO_2 photocatalysts in presence of various kinds of reactant molecules has already been investigated [36]. PL intensity dependence on atmosphere was explained in terms of surface band bending of titania particles.

The PL measurements were performed to analyse the photogenerated carrier separation efficiency of the doped samples. PL emission intensity of a semiconductor is proportional to the photoinduced electron-hole recombination rate. TiO_2 is a semiconductor with an indirect band gap. Titania exhibits a broad visible luminescence spectrum, which is related to transition of a trapped charge carrier in the oxygen vacancy to the TiO_2 valence band [37].

All samples were photoexcited by a light at wavelength 325 nm. It corresponds to photon energy of 3.81 eV, which is higher than the band gap energy of titania. This energy is absorbed by exciting transition of valence band electrons to the conduction band. The PL spectra of the initial TiO_2 P 25 Degussa and P25-u are displayed in Fig. 5. Intensive peaks in the spectrum of TiO_2 P 25 Degussa with maxima in the blue region at about 416 nm (2.98 eV) and 464 nm (2.67 eV) can be ascribed to emission of a photon having a slightly lower energy than the band gap width of the anatase and rutile phases in P25 TiO_2. This is evidence for direct recombination of a photoexcited electron and a positively charged hole [38−39]. A contribution of rutile particles of sample P25 to the excitation band is higher than that of anatase [40]. Rutile particles of sample P25-u have lower photoluminescence efficiency than the initial P25. A charge transfer between the anatase and rutile phases can explain this. Some electrons in the anatase particles that are excited from the valence band to the conduction band are transferred to the rutile particles because the energy level of conduction band in anatase particles is higher than that in the rutile entities [41]. The peak at 464 nm in the visible region is attributed to defects in the samples, namely the oxygen-ion vacancies, which provide acceptor levels near the conduction-band edge [42].

In the mechanochemically prepared P25-u sample, PL emission peaks were observed within blue (370−480 nm) and green (490−565 nm) regions. In the blue region, a peak at 404 nm and shoulders at 416 and 366 nm were registered that are characteristic of rutile and anatase phases, respectively. The peak at 404 nm in PL spectrum of P25-u sample is attributed to emission of band gap transition [43] and arises from radiative annihilation of excitons (band to band recombination) [44]. The intensity of PL signal for P25-u was lower than that of P25 sample. The differences are due to a different content of defects and/or oxygen vacancies by preparation methods. This demonstrates the fact that co-

existence of rutile and anatase phases is responsible for changes in PL intensity and superior photocatalytic activity of the N-doped P25-u samples. In addition, a low intensity emission peaks appeared at higher wavelengths of 464 and 530 nm. In the observed PL spectra, the peak at 464 nm is related to self-trapped excitons (STE) and a peak at 530 nm is associated with oxygen vacancies [45]. We suppose that band-band PL emissions of heterojunctions were broadened due to nanocrystalline nature and mixed contribution from individual rutile-anatase phases.

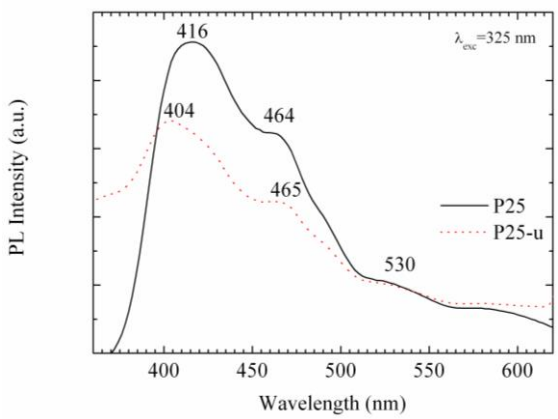

Fig. 5. Photoluminescence spectra of P25 (1) and P25-u (2) samples.

Photocatalytic properties

The photocatalytic activity of mechanochemically synthesised samples was evaluated by degradation of representative industrial dye Methyl Orange in aqueous solution under visible irradiation. All experiments were performed under room temperature. For comparative purpose, the activity of TiO_2 P25 Degussa was also investigated under the same conditions. Temporal changes in the concentration of MO were monitored by examining the variation in maximal absorption in UV-vis at 464 nm.

In a region where Lambert-Beer law is valid the concentration of MO dye is proportional to the absorbance as shown in Fig. 6. It can be seen that P25 demonstrated the smallest adsorption of MO (only 1%), while the P25-u sample showed a higher value (3%). It has been documented that preliminary adsorption of dye on the photocatalytic surface is a prerequisite for highly efficient oxidation [46]. The photocatalytic efficiency (C/C_o) in presence of P25 and P25-u photocatalysts is represented on Fig. 6 where C_o is the initial concentration of MO. Based on blank experiments self-photolysis of MO could be neglected. TiO_2 P25 Degussa was taken as reference for comparison and in this case, the MO degradation was about 2% after 120 min. The P25-u sample manifested higher photodegradation activity with a MO conversion of 60% after 120 min irradiation. As shown in Fig. 6, the photocatalytic degradation curves of MO followed a pseudo-first order kinetic model, as given in Eq. 4:

$$\ln (C_o/C_t) = k't, \quad (4)$$

where: k' (min^{-1}) is the reaction rate constant, C_o is the initial MO concentration, and C_t is the MO concentration at a certain time (min). The reaction rate constant k could be estimated from Eq. 4 by plotting $\ln(C_o/C_t)$ versus irradiation time. Values of the reaction rate constant are presented in Table 1.

The reaction rate constant of the mechanochemically synthesised P25-u sample was higher than that of initial P25 (0.094 min^{-1}). Enhanced photocatalytic activity of the mechanochemically prepared P25-u samples containing anatase and rutile phases is due to difference in conducting band edges of the anatase and rutile phases. This may promote interfacial electron transfer from rutile to anatase and resulting energy barrier would suppress back electron transfer, which decreases the probability of the charge carrier recombination, confirmed by the low PL intensity (see Fig. 5).

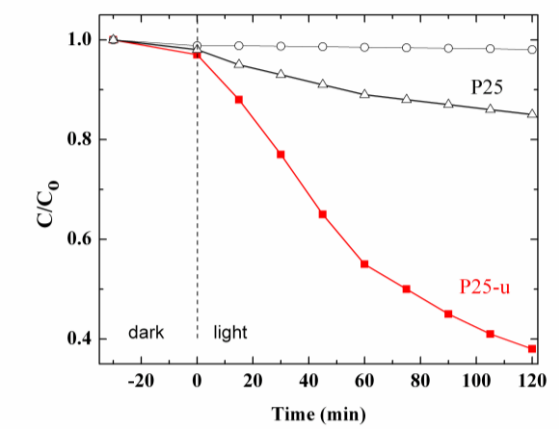

Fig. 6. Photodegradation of MO as a function of irradiation time of blank experiment without photocatalyst (○), commercial P25 (Δ) and mechanochemically synthesized sample P25-u (■).

Photocatalysis is a process, which depends on numerical parameters such as particle size, porous structure, crystallinity, surface area, and dopant. The presence of mixed phase improves the photochemical performance of the samples through reducing the recombination of photogenerated holes and electrons.

CONCLUSIONS

An eco-friendly one-step mechanochemical method to prepare N-doped TiO_2 samples for efficient photocatalytic decolourisation was established. During the mechanical activation, a transformation of anatase to rutile was established. Whereas the

initial P25 contained mainly big mesopores and macropores, the P25-u samples were almost completely mesoporous. A broadened absorption edge and a narrowed energy band gap were observed. The results show that titania phase composition is an important factor determining the PL intensities and photocatalytic activity in photodecolourisation of Methyl Orange of the mechanochemically synthesised samples.

Acknowledgment: *The authors are grateful to the Bulgarian Science Fund for financial support by project DNTS/Slovakia 01/2 and to the Slovak Research and Development Agency under the contracts SK-BG-2013-0011 and 14-0103. M.F. and E.D. thank VEGA (project 2/0128/16 and 2/0065/18). M.B. acknowledges the support of Slovak Grant Agency VEGA (project 2/0044/18).*

REFERENCES

1. M. R., Hoffmann, S. T. Martin, W. Y. Choi, D. W. Bahnemann, *Chem. Rev*., **95,** 69 (1995).
2. R. Marschal, L. Wang, *Catal. Today*, **225,** 111 (2014).
3. Y. Hu, H. Liu, X. Kong, X. Guo, *J. Nanosci. Nanotechnol.,* **14**, 3532 (2014).
4. M. Kitano, K. Funatsu, M. Matsuoka, M. Ueshima, M. Anpo, *J. Phys. Chem*, C, **110**, 25266 (2006).
5. L. Youssef, A. J. K. Leoga, S. Roualdes, J. Bassil, M. Zakhour, V. Rouessac, A. Ayral, M. Nakhl, *J. Eur. Ceram. Soc.*, **37**, 5289 (2017).
6. S. Yang, L. Gao, *J. Amer. Ceram. Soc.*, **87,** 1803 (2004).
7. T. Sano, N. Degushi, T. Takeshi, S. Matsuzawa, *J. Mater. Chem.*, **14,** 380 (2004).
8. G. Liu, X. Wang, L. Wang, Z. Chen, F. Li, G. Lu, H.-M. Chen, *J. Coll. Interface Sci*., **334**, 171 (2009).
9. S. Livraghi, A. M. Czoska, M. C. Paganini, E. Giamello, *J. Solid. State Chem*., **182**, 160 (2009).
10. K. Kobayakawa, Y. Murakami, Y. Sato, *J. Photochem. Photobiol. A: Chemistry*, **170**, 177 (2005).
11. T. Ohno, K. Sarukawa, K. Tokieda, M. Matsumura, *J. Catal*., **203**, 82 (2001).
12. M. Anpo, *Bull. Chem. Soc. Jpn*, **77**, 1427 (2004).
13. U., Stafford, K. A. Gray, P. V. Kamat, A. Varma, *Chem. Phys. Lett*., **205**, 55 (1995).
14. G. Riegel, J. R. Bolton, *J. Phys. Chem.*, **99**, 4215 (1995).
15. R. P. Busca, J. Kiwi, *Appl. Catal. B-Environ.*, **16**, 19-(1998).
16. S. M. El-Sheikh, T. M. G. Zhang, V. Vogiazi, A. A. Ismail, K. O'Shea, D. D. Dionysiou, *Chem. Eng. J*. **310,** 428 (2017).
17. Z. C. Orel, M. K. Gunde, B. Orel, *Prog. Org. Coat.*, **30**, 59 (1997).
18. N. G. Kostova, E. Dutkova, *Bulg. Chem. Commun*., **46**, Special issue C, 87 (2015).
19. S. Begin-Colin, T. Girot, *J. Solid State Chem*., **149**, 41 (2000).
20. H. Zhang, J. F. Banfield, *J. Phys. Chem*. B, **104**, 3481 (2000).
21. A. L. Patterson, *Phys. Rev*., **56,** 978 (1939).
22. J. Z. Niu, W. W. Xu, H. B. Shen, S. Li, H. Z. Wang, L. S. Li, *Korean Chem. Soc*., **33**, 393 (2012).
23. P. Baláž, M. Achimovičová, M. Baláž, P. Billik, Z. Cherkezova-Zheleva, J. M. Craido, F. Delogu, E. Dutková, E. Gaffet, F. J. Gotor, R. Kumar, I. Mitov, T. Rojac, M. Senna, A. Streletskii, K. Wieczorek-Ciurowa, *Chem. Soc. Rev*., **42**, 7571 (2013).
24. S. J. Xiong, Y. Tang, H. S. Ng, X. Zhao, Z. Jiang, Z. Chen, K. W. Ng, S. C. J. Loo, *Toxicology*, **304**, 132 (2013).
25. W. Li, C. Ni, H. Lin, C. P. Huang, S. Ismat Shah, *J. Appl. Phys*., **96**, 6663 (2004).
26. P. Dulian, M. Buras, W. Zukowski, *Polish J. Chem. Technol*., **18**, 68 (2016).
27. K. S. W. Sing, D. H. Everett, R. A. W. Haul, L. Moscou, R. A. Pierott, J. Rouquerol. T. Sieminiewska, *Pure Appl. Chem.*, **57**, 603 (1985).
28. V. Nadtochenko, N. Denisov, A. Gorenberg, Yu. Kozlov, P. Chubukov, J. A. Rengifo, C. Pulgarin, J. Kiwi, *Appl. Catal. B-Environ*., **91**, 460 (2009).
29. S. Ardizzone, C. L. Bianchi, G. Cappelleti, S. Gialanella, C. Parola, V. Ragaini, *J. Phys. Chem*. C, **111,** 13222 (2007).
30. E. McCafferty, J. P. Wightman, *Surf. Interface Anal*. **26**, 549 (1998).
31. W. Zhang, Y. Li, S. Zhu, F. Wang, *Chem. Phys. Lett*. **373**, 333 (2003).
32. T. Tsoncheva, R. Ivanova M. Dimitrov, D. Paneva, D. Kovacheva, J. Henych, P. Vomacka, M. Kormunda, N. Velinov, I. Mitov, V. Stengl, *Appl. Catal. A:* General, **528**, 24 (2016).
33. R. Asahi, T. Morikawa, T. Ohwaki, K. Aoki, Y. Taga, *Science*, **293**, 269 (2001).
34. M. Hamadanan, A. Reisi-Vanani, A. Majedi, *Mater. Chem. Phys.*, **116**, 376 (2009).
35. S. G. Kumar, L.G. Devi, *J. Phys. Chem*. A **115**, 13211 (2011).
36. M. Anpo, M. Che, *Adv. Catal*., **44,** 119 (2000).
37. M. Tahir, N. S. Amin, *Appl. Catal. B. Environ*., **162**, 98 (2015).
38. S. Liu, X-J. Zhao, Q. Zhao, X. He, J. Feng, *J. Electron Spectrosc. Relat. Phenom.,* **148**, 158 (2005).
39. D. Dastan, P. U. Loundhe, N. B. Chaure, *Mater. Sci.-Mater. Electr*., **25**, 3473 (2014).
40. H. Nakajama, T. Mori, Q. Shen, T. Toyada, *Chem. Phys. Lett*., **409**, 81 (2005).
41. J. Yu, J. C. Yu, W. Ho, Z. Jiang, *New J. Chem.* **26,** 607 (2002).
42. J. Liqiang, Q. Yichun, W. Baiqi, L. Shudan, J. Baojiang, *Sol. Energy Mater. Sol. Cell*., **90,** 1773 (2006).
43. K. L. L. Li, *J. Mol. Catal.* A, **356**, 78 (2012).
44. J. Xu, L. Li, *J. Colloids Interface Sci.*, **318**, 29 (2008).
45. J. Preclikova, P. Galar, *J. Appl. Phys*., **108**, 113502 (2010).
46. Y. M. Xu, C. H. Langford, *Langmuir*, **17**, 897 (2001).

ОХАРАКТЕРИЗИРАНЕ НА МЕХАНОХИМИЧНО СИНТЕЗИРАН ДОТИРАН С АЗОТ TiO_2

Н. Г. Костова*,[1], М. Фабиан[2], Е. Дуткова[2], М. Балаж[2], М. Шипочка[3]

[1] *Институт по катализ, Българска академия на науките, 1113 София, България*
[2] *Институт по геотехника, Словашка Академия на науките, 04001 Кошице, Словакия*
[3] *Институт по неорганична химия, Българска академия на науките, 1113 София, България*

Постъпила на 29 януари 2018 г.; Преработена на 20 март 2018 г.

(Резюме)

Дотиран с азот TiO_2 фотокатализатор (P25-u) е получен чрез комбиниран механохимичен/термичен синтез. Като източник на азот е използван карбамид. Опитите с влажно смилане бяха проведени с титанов диоксид P25 Дегуса във високоенергийна планетарна мелница. След смилане образецът беше накален при 400 °C. Образците са охарактеризирани с помощта на рентгенов фазов анализ (РФА), азотни адсорбционни-десорбционни изотерми, ултравиолетова-видима дифузионно-отражателна спектроскопия (ДОС), рентгенова фотоелектронна спектроскопия (РФЕС) и фотолуминесцентен спектроскопски (ФС) анализ. Резултатите от рентгенофазовия анализ показаха, че част от фазата анатаз се трансформира в рутил по време на влажното смилане. Всички дифракционни линии бяха уширени, което свидетелства, че размерът на кристалитите е в нанометричната област. Образецът P25-u показа по-ниска специфична повърхност от тази на изходния образец P25 Дегуса. Смилането във влажна среда довежда до влошаване на порестата структура на образеца. По-ниският интензитет на фотолуминесцентния спектър на механохимично синтезирания образец P25-tu в сравнение в изходния P25 свидетелства за по-ниска скорост на рекомбиниране на фото-възбудените електрони и дупки. Определена беше стойността на енергията на забранената зона E_{bg} на образеца P25-u (2.36 eB). Този резултат навежда на мисълта за възможното приложение на така получения материал като фотокатализатор в процеса на разграждане на багрила чрез облъчване с видима светлина. Механохимично синтезираният дотиран с азот титанов диоксид с прекурсор карбамид показа по-висока скорост на обезцветяване на багрилото Метил Оранж при облъчване с видима светлина в сравнение с търговския прахообразен TiO_2 Дегуса.